

Original Research

Removal of Crystal Violet and Eriochrome Black T Dyes from Aqueous Solutions by Magnetic Nanoparticles Biosynthesized from Leaf Extract of *Fraxinus Chinensis Roxb*

Imran Ali^{1,2}, Changsheng Peng^{1-3*}, Zahid M. Khan⁴, Muhammad Sultan^{4**}, Iffat Naz⁵, Mohsin Ali⁶, Hafiz U. Farid⁴, Muhammad H. Mahmood⁴, Rameez Ahsen⁴

¹Department of Environmental Engineering, College of Environmental Science and Engineering, Ocean University of China, Qingdao, China

²The Key Lab of Marine Environmental Science and Ecology, Ministry of Education, Ocean University of China, Qingdao, China

³School of Environmental and Chemical Engineering, Zhaoqing University, Zhaoqing, China

⁴Department of Agricultural Engineering, Bahauddin Zakariya University, Multan, Pakistan

⁵Department of Biology, Qassim University, Buraidah, Kingdom of Saudi Arabia

⁶Department of Environmental Engineering, Middle East Technical University, Ankara, Turkey

Received: 4 January 2018

Accepted: 25 March 2018

Abstract

In the present research, a “green” recipe was used to produce innovative phyto-genic magnetic nanoparticles (PMNPs) from leaf extract of *Fraxinus chinensis Roxb* without employing any additional toxic surfactants as capping agents. The convenient reaction between metal salt solution and plant biomolecules occurred within a few minutes by color changes from pale green to intense black, hinting at the production of magnetic nanoparticles (MNPs). The formation of PMNPs was verified by employing different techniques such as UV-visible spectrophotometry, Fourier transform infrared spectroscopy (FTIR), powder X-ray diffraction (XRD), scanning electron microscope (SEM) and energy dispersive X-ray (EDX). The fabricated PMNPs were further utilized as a catalyst for removing toxic dyes, i.e., Crystal violet (CV) and Eriochrome black T (EBT) from aqueous solutions in the presence of hydrogen peroxide (H₂O₂). The concentrations of CV and EBT were calculated using ultraviolet-visible (UV-vis) spectroscopy throughout all the experiments. The results indicated that PMNPs showed >95% removal of both dyes within 10 min of contact time over a wide range of concentration, 10-300 mg/L. The degradation kinetics were also investigated using first- and second-order rate equations, and the results indicated that kinetic data of both CV and EBT followed first-order degradation rate. Moreover, the removal efficiency of the fabricated PMNPs was also

*e-mail: pcs005@ouc.edu.cn

**e-mail: muhammadsultan@bzu.edu.pk

compared with chemically synthesized magnetic nanoparticles (CSMNPs), and the results indicated that our fabricated PMNPs were more effective in terms of extent and speed to remove dyes. Finally, we have also proposed a possible removal mechanism. Altogether, the developed “green” recipe can easily be implemented to produce potentially biocompatible and non-toxic PMNPs for treatment of wastewater and can also easily be employed in low-economy countries.

Keywords: *Fraxinus chinensis* Roxb, plant leaf extract, phytogetic magnetic nanoparticles, Crystal violet, Eriochrome black T

Introduction

Water pollution levels of natural streams is increasing day by day due to the discharge of toxic dyes and aromatic pollutants from different industries like leather, cosmetics, textile, food and pharmaceuticals, etc. [1-5]. Out of all industries, the textile industry mainly uses toxic dyes for coloring their products and discharging a huge amount of toxic dyes contaminated into the natural/aquatic environment without proper treatment. Thus, worldwide the annual production of dyes is approximately 0.7 million tons and the textile industry generates huge quantities of complex chemical substances as waste, including dyes in the form of wastewater in various stages of textile manufacturing and processing. On average, to produce 1 kg of textile, ~200 L of water is consumed and an average-sized textile mill with a production of about 8000 kg of fabric per day consumed about 1.6 million L water. Moreover, on average, the reported concentrations of biological oxygen demand (BOD_5), total solids (TS) and color in textile wastewater are about 6000, 1560 mg/L and 1450-4750 ADML, respectively [6-8]. Importantly, these toxic dyes are creating harmful effects and diseases in residential communities, i.e., allergies, jaundice, heart defects, skin irritation, and tumors. In addition, these toxic dyes are destroying aquatic life by creating a hindrance to penetration of proper sunlight for photosynthesis due to having visible color [9-11]. Therefore, the removal and treatment of these dyes is an important area of applied research for wastewater treatment experts to keep natural water environments safe and clean.

The conventional biological methods (such as trickling filter, activated sludge system, membrane bioreactors, etc.) and chemical treatment methods (such as coagulation, flocculation, electrochemical oxidation, etc.) are often considered ineffective and expensive for the treatment and handling of these toxic dyes, because these toxic dyes usually show resistance to aerobic biodegradation, heat, oxidizing agents and light [3, 1, 12]. In contrast, adsorptive treatment is normally considered an alternate option to treat such toxic and aromatic pollutants because of their design simplicity, treatment flexibility and insensitivity to toxicity. For this purpose, the removal performance of different adsorbents, including agricultural wastes – such as banana pith, orange peel [13], rice husk [14],

peanut hull [15], coir pith [16], pinewood and jute fiber [17] – activated carbon and its different composites have been well documented. For instance, Sivaraj et al. [13] used orange peel as an adsorbent to remove Acid violet 17 from aqueous solutions and reported a maximum of 87% removal and 19.88 mg/g adsorptive capacity at an adsorbent dose of 600 mg/50 mL using 10 mg/L of initial dye concentration. Similarly, Gong et al. [15] reported the use of powdered peanut hull as an adsorbent to remove three anionic dyes such as amaranth (Am), sunset yellow (SY) and fast green FCF (FG). The findings of this study revealed that a maximum of 14.9, 13.9 and 15.60 mg dye per gram of the adsorptive capacity was achieved for Am, SY and FG, respectively, using adsorbent dose of 5.0 g/L. In another study jute fiber carbon (JFC) was used as a low-cost adsorbent material and it showed the removal of 92.06% of eosin yellow, 87.65% of malachite green (MG) and 95.93% of crystal violet from aqueous solutions [17]. However, certain issues such as low removal capacity and lack of reusability are hindering its execution for real applications.

Hence, in order to handle these issues and improve their performance, nanostructured metal oxide and its composites are getting great research attention due to their easy fabrication, low cost requirement, high stability, high magnetic permeability and ease in separation from the final effluents by applying an external magnetic force [18-19]. They have been utilized for the removal and degradation of toxic and aromatic pollutants from wastewaters due to their unique physical, chemical and catalytic characteristics. For example, Luo and Zhang [19] fabricated cellulose-based magnetic beads by incorporating activated carbon (AC) for the removal of methyl orange (MO) and methylene blue (MB) from aqueous solution. The findings depicted more than 95% removal of both dyes observed within the contact time of 180 min and prepared material separated from solution just by applying a magnet, and reused for at least 3 times by retaining removal efficiency above 95%. Similarly, green magnetic nanoparticles were also employed for the removal of toxic dyes as explained in detail in the author’s previously published report [2]. Until now, different methods (hydrothermal process, electrochemical route, chemical co-precipitation, sol-gel technique, and micro-emulsion technique) have been documented in literature to fabricate/synthesize these metal oxide nanoparticles [3-5]. However, certain

aspects such as the requirement of high temperature and pressure, involvement of hazardous and toxic reducing and capping agents to stabilize the size and composition of magnetic nanoparticles, and the harsh reaction conditions and long reaction time are the main disadvantages of employing these fabrication methods [2-5]. In addition, the aggregation of these nanoparticles into chain-like structures was one of the well-known characteristics, which was responsible to reduce its surface area-to-volume ratio [20]. However, it is also worth mentioning here that the stability of these nanoparticles against aggregation can be enhanced by utilizing organic surfactants or through the use of different capping agents [21].

Another approach that can serve this goal is to fabricate iron oxide nanoparticles using green nanotechnology [22]. Green nanotechnology is getting great research interest because of its low cost, involvement of plant bio-molecules as reducing and capping agents instead of toxic and hazardous chemicals, and requirement of low temperature and pressure to fabricate metal oxide NPs [23]. In addition, green fabrication would impart steric stabilization of iron NPs against aggregation and help to minimize the concerns related to the use of toxic and hazardous chemicals (sodium borohydride, NaBH_4) as a reducing agent because this chemical is famous for its corrosiveness and flammability. Recently, different kinds of plant leaves, flowers and fruit peels have been employed for the fabrication of metal oxide NPs, and their adsorptive and catalytic performance have also been documented in the literature [4]. Moreover, it can be observed from the published reports that mostly green magnetic nanoparticles (MNPs) have been used for the adsorptive removal of heavy metals ions (Pd, Cd, Hg, As and Cr) from aqueous solutions [24-30]. However, very limited literature is available to address its catalytic performance to degrade toxic dyes and aromatic pollutants [31-33]. For instance, Buazar et al. [31] conducted a study to remove an organic methylene blue (MB) contaminant from wastewater at room temperature using green MNPs fabricated by homemade starch-rich potato extract and reported 100% removal of MB from solutions within the contact time of 30 min. Similarly, another study showed malachite green (MG) dye 96% removal efficiency within the contact time of 60 min at 50 mg/L and 298K by using green iron NPs synthesized from green tea extract [33]. Recently, Prasad et al. [32] investigated the degradation of Methyl orange (MO) dye from aqueous solution using Fe_3O_4 magnetic nanoparticles (MNPs) fabricated from extract of *Pisum sativum* peels (PS), and reported 96% removal within the contact time of 60 min at concentration of 100 mg/L. Therefore, in the present study, we employed our fabricated green MPNs for the catalytic degradation of cationic CV and anionic EBT toxic dyes to investigate the influence of different kinds of dyes on the degradation performance by green MNPs.

Herein, we fabricated for the first time, phylogenetic magnetic nanoparticles (PMNPs) from leaf extract of *Fraxinus chinensis Roxb* as a reducing and capping agent for the degradation of toxic dyes. The common name of *F. chinensis Roxb* plant is Chinese ash. Its leaves have been used in traditional Chinese medicine (TCM) for dysentery disorders. The genus is widespread across much of Europe, Asia and North America. Its growth rate in the city of Qingdao, China is very high and its leaves are easily available without any costs or/ nominal price. The main objectives of the current study was (i) to fabricate PMNPs using leaf extract of *F. chinensis Roxb*; (ii) to confirm the fabrication by using different techniques such as UV-visible spectrophotometry, fourier transforms infrared spectroscopy (FT-IR), powder X-ray diffraction (XRD), scanning electron microscope (SEM) and energy dispersive X-ray (EDX); (iii) to investigate the effectiveness of PMNPs to remove toxic dyes (i.e., CV and EBT) from aqueous solutions in the presence of H_2O_2 ; and (iv) to compare the performance of PMNPs with chemically synthesized magnetic nanoparticles (CSMNPs) in terms of extent and speed to remove toxic dyes by fitting experimental data into first- and second-order rate equations.

Materials and Methods

Materials and Chemicals

Various different chemicals – viz., Ferric chloride hexahydrate ($\text{FeCl}_3 \cdot 6\text{H}_2\text{O}$), ferrous sulfate ($\text{FeSO}_4 \cdot 7\text{H}_2\text{O}$), sodium hydroxide (NaOH), tripyridyltriazine (TPTZ, HPLC grade), acetate buffer, HCl, ferric trichloride, potassium ferricyanide, copper sulfate, Na_2CO_3 , MgSO_4 , crystal violet ($\text{C}_{25}\text{H}_{30}\text{ClN}_3$), NaBH_4 (Aldrich, 99%), Eriochrome black T ($\text{C}_{20}\text{H}_{12}\text{N}_3\text{O}_7\text{SNa}$) (Aldrich, 99%), ethanol ($\text{C}_2\text{H}_5\text{OH}$), gallic acid (Merck, 99.9%), H_2O_2 (Aldrich, 30%), ethanol ($\text{C}_2\text{H}_5\text{OH}$), and gallic acid (Merck, 99.9%) – were used without further purification in the present research investigation. Deionized water (DI) was obtained from the Qingdao Water Purification Agency to make all aqueous solutions. For making CV and EBT stock solution (1000 mg/L), 1000.0 mg powder chemical of CV and EBT was added in 1000 mL DI water in the volumetric flask. Furthermore, different concentrations of dye solutions were prepared using dilution method ($C_1V_1=C_2V_2$) by keeping the volume of dyes solution constant (50 mL). The pH adjustments were made by using 0.1 mol/L NaOH and HCl solution throughout all the experiments, wherever needed.

Biosynthesis of Phylogenetic Magnetic Nanoparticles (PMNPs)

Selection of Fraxinus chinensis Roxb

For the fabrication of PMNPs, the leaves of '*F. chinensis Roxb*' were selected and were washed

with DI water to remove impurities (dust), then dried under sunlight for at-least 10 days and further kept in a drying oven for 6 h at 85°C to reduce moisture. Then the dried plant leaves were chopped into small pieces manually and passed through a 2 mm sieve. The final product was collected and stored for further use in the preparation of extract.

Evaluating the Reducing Capacity of the Extracts

The reducing ability of the extract was investigated using ferric reducing antioxidant power (FRAP) assay and color development tests [34]. During the FRAP assay, the ability of the extract to reduce Fe^{+3} to Fe^{+2} is measured at absorbance ($\lambda = 593$ nm) by producing blue complex with tripyridyltriazine (TPTZ). The FRAP reagent was made by using 20 mM of FeCl_3 solution, 300 mM of acetate buffer and 10 mM of TPTZ solution in HCl at a 1:1:10 ratio. The absorbance of samples containing 800 μL of FRAP reagent, 60 μL of H_2O , and 20 μL of extract was determined at $\lambda = 593$ nm using a UV-vis spectrophotometer. The FRAP reagent was kept at room temperature (25°C) throughout the experiments [35]. The standard calibration curve for this test was also designed using six Fe^{+2} standards with concentration range between 100 and 1000 $\mu\text{mol/L}$ ($r > 0.999$), which was further used in extract optimization study.

Total Phenolic Content (TPC)

The presence of phenolic compounds is often considered an important element in the formation of green MNPs, because it has been reported that phenolic compounds with -OH groups in the orthoposition assist in the reduction and construction of green magnetic nanoparticles [36]. For this purpose, the Folin-Ciocalteu method was employed to investigate TPC in the extract using gallic acid as the standard [34]. A dilution sample was prepared containing extract (20 μL) and 40 μL of pure DI water. Thereafter, Folin-Ciocalteu reagent (100 μL) was added and mixed. After mixing of 5 min, 300 μL of Na_2CO_3 solution was injected and permitted to stand for 15 min. Finally, the absorbance of the sample was determined at $\lambda =$ by UV-vis spectrophotometer. The results of TPC were stated as milligrams of gallic acid equivalent (GAE) per gram of dry weight.

Fabricating Phytogetic Magnetic Nanoparticles (PMNPs)

The optimized extraction condition and fabrication protocol was selected and employed for the fabrication of PMNPs. Briefly, for preparing extract, 10 g of leaf powder of *F. chinensis Roxb* was added in 80 mL of DI and the mixture was heated at 80°C for 90 min.

The pH of the solution was maintained at 3 using 0.1 mol/L NaOH and HCl solution. Thereafter, (1:1) metal solution (MS) ratio of (Fe^{+2} : Fe^{+3}) was prepared using 50 mL DI. After this, 50:50 (vol./vol.) ratio of MS and extract was prepared and boiled at 80°C with continues stirring (at 100 rpm) by a magnetic stirrer heater for 60 min. The pH of the mixture was adjusted at 12 by adding 0.1 mol/L NaOH solution drop-wise. The mixture color was changed from reddish brown to black, indicating the formation of PMNPs. Then the mixture was allowed to stand for 60 min and the black color precipitations were centrifuged for 20 min at 8000 rpm, then the supernatant was vacuum-filtered through a 0.22 μm filter paper. The black powder was collected and washed twice with 50 mL of ethanol solution. The final product was again vacuum-filtered through a 0.22 μm filter paper. Lastly, the collected black powder was kept in a drying oven for at least 120 min at 80°C. The obtained PMNPs were further employed in degradation experiments.

Fabricating Chemically Synthesized Magnetic Nanoparticles (CSMNPs)

For performance comparison, the CSMNPs were fabricated by chemical co-precipitation method using sodium borohydrate (NaBH_4) as a reducing agent. Briefly, first MS 2:1 ratio of $\text{FeCl}_3 \cdot 6\text{H}_2\text{O}$ (18.965 g) and $\text{FeSO}_4 \cdot 7\text{H}_2\text{O}$ (9.563 g) was added in 50 mL solution of (90%) ethanol absolute and the mixture was boiled at 80°C with continuous stirring (100 rpm) by a magnetic stirrer heater. Meanwhile, 80 mL of NaBH_4 solution was prepared separately using 8.23g of NaBH_4 . Thereafter, NaBH_4 solution was injected drop-wise (25-45 drop/min) in the first solution. The black color precipitations appeared quickly, when the first drop of NaBH_4 solution was injected. Thereafter, NaBH_4 solution was injected drop-wise until metal solution color was completely changed from reddish yellow to black. The mixture was allowed to heat for 1.0 h. Finally, after settling for 1.0 h, the mixture was vacuum-filtered through a 0.22 μm filter paper. The black powder was collected and washes twice with 50 mL of ethanol solution. The final product was again vacuum-filtered through a 0.22 μm filter paper. Thereafter; the collected black powder was kept in a drying oven at 80°C for 60 min. These CSMNPs were further employed for degradation experiments.

Characterization

Characterization of Plant Extract

Elemental contents (C, N, S and H) and heavy metals content of plant leaves extract were determined by using elemental analyzer (EA, Vario EL cube, German) and atomic absorption spectrometry (Solar M6, Thermo Elemental, USA), respectively.

Characterization of Phylogenetic Magnetic Nanoparticles (PMNPs)

The fabricated PMNPs were characterized using FTIR, XRD, SEM and EDX/S, techniques. A Bruker Vertex 70 was used for FTIR analysis and the probable bio-molecules present in the plant extract were identified, which were responsible for the reduction and stabilization of PMNPs. A Philips Electronic Instrument was employed for the XRD analysis and the crystalline shape of the fabricated PMNPs and CSMNPs was identified. The fabricated PMNPs and CSMNPs samples were washed completely with ethanol prior to analysis in order to minimize the NaCl content and other impurities that crystallized during the fabrication process. The samples were scanned within 2θ range of $20-70^\circ$. The morphologies of the fabricated CSMNPs and PMNPs were scrutinized by scanning electron microscopy (SEM) and the elemental content was analyzed by energy dispersive spectroscopy EDS/X (SEM/EDX, JSM-6700F).

Batch Experiments

For the removal investigation, batch experiments were performed by shaking Erlenmeyer flasks in a thermostat water bath under atmospheric pressure and room temperature ($25\pm 2^\circ\text{C}$). A fixed amount of 0.500 g powdered PMNPs and CSMNPs was added in each dye solution along-with 2 mL of (30%) H_2O_2 solution and the shaking speed was kept constant at 100rpm for all the experiments. The pH of the dye solution was adjusted at 6.5 using 0.1 mol/L NaOH and HCl solution, similar to real acid dyeing effluents, unless otherwise stated. For checking the influence of dyes concentration on the removal performance, the concentration of the dyes solution was varied from 10-300 mg/L in a 100 mL Erlenmeyer flask (where the total volume of the dye solution was 50 mL along with 2 mL of 30% H_2O_2 solution). At the end of the each experiment, the PMNPs and CSMNPs were separated by using a magnet, and the final solutions were vacuum-filtered through $0.45\mu\text{m}$ filter paper. The final dye concentration values were determined using UV-vis spectrophotometer and samples absorbance readings were calculated at $\lambda_{\text{max}} = 585 \text{ nm}$ for Crystal violet (CV) and $\lambda_{\text{max}} = 623 \text{ nm}$ for Eriochrome black T (EBT). The predetermined standard calibration curves were employed to measure the actual dyes concentration. All the experiments were performed in triplicate and the average values were used to make the final discussion. Finally, the removal efficiency at different dosages and dye concentrations was calculated as:

$$\text{Removal efficiency (\%)} = \frac{C_o - C_t}{C_o} \times 100\%$$

...where C_o (mg/L) is the initial dye concentration in the solution and C_t (mg/L) is the final concentration dye solution at different time intervals.

For kinetic studies, a fixed amount of 0.500 g powdered PMNPs and CSMNPs were added in an Erlenmeyer flask containing 2 mL of 30% H_2O_2 solution and 48mL of 300 mg/L dye solutions. The mixture was placed in a thermostat water bath under atmospheric pressure and room temperature ($25\pm 2^\circ\text{C}$) by adjusting shaking speed at 100 rpm. The aqueous dyes concentration was determined at the end of 5, 10, 15, 20, 30, 60, 120, 180, 240, 300 and 360 min. At the end of the each experiment, PMNPs and CSMNPs were separated using a simple magnet and the final solutions were vacuum-filtered using $0.45\mu\text{m}$ filter paper. Then the UV-vis absorbance values were measured using a UV-Vis spectrophotometer. All the kinetic experiments were conducted in triplicate and the average values were put in the kinetic equations given below [20]:

First-order rate equation

$$\ln\left(\frac{C_t - C_e}{C_o - C_e}\right) = -k_1 t$$

Second-order rate equation

$$\frac{1}{C_t - C_e} - \frac{1}{C_o - C_e} = k_2 t$$

...where C_o (mg/L) is the initial concentration of the dye solution, C_t (mg/L) and C_e (mg/L) are the concentrations at time (t) and equilibrium, and k_1 and k_2 are the rate constant for 1st and 2nd equations.

Results and Discussion

Characterization of Leaf Extracts of *F. chinensis Roxb*

The main objective of the extract characterization was to examine the safe and clean green synthesis of PMNPs by investigating the elemental contents and heavy metals content. The surplus amount of heavy metals can generate contamination in the plant leaf extract. In addition, it has been reported that by knowing elemental contents (C, H, N and S), the probability regarding the presence of certain organic compounds can be supposed. In the present study, the elemental contents of *F. chinensis Roxb* were C (38.6%), H (4.99%), S (0.39%) and N (4.38%). Hence, these results indicated that the presence of N and S might be due to protein, chlorophyll, nucleic acids, cysteine, cystine and methionine in the plant leaf extract. In contrast, negligible contents of heavy metals Cr (0.011 mg/L), Fe (0.06 mg/L), Pb (0.07 mg/L), Co (0.013 mg/L), Cd (0.001 mg/L), and Zn (0.25 mg/L)

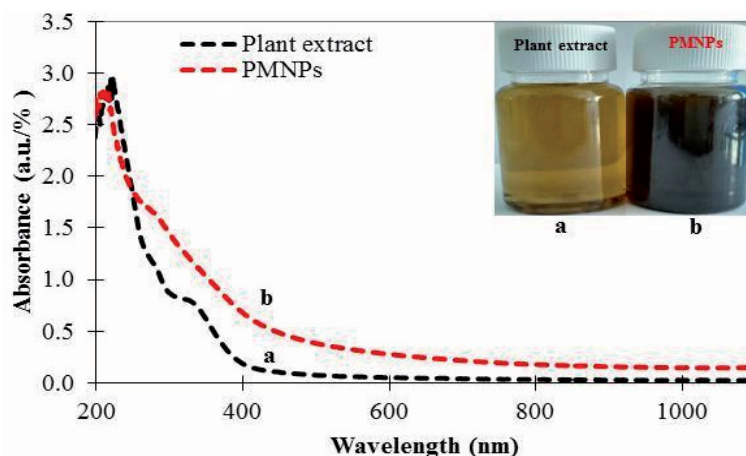


Fig. 1. UV-vis spectra of *F. chinensis* Roxb leaf extract a) and phylogenetic magnetic nanoparticles (PMNPs) b); inset shows the photographic interpretation of the reaction [34].

were observed in the extract. Our finding indicated that organic compounds were the main component of this extract and only negligible amounts of heavy metals contents were observed, thereby confirming safe and green fabrication of PMNPs. Furthermore, it was also noticed that at optimized conditions, higher antioxidant capacity ($0.047 \text{ Fe}^{+2} \text{ mmol/L}$) and TPC ($83.3 \pm 5.1 \text{ GAE mg/g DW}$) was measured by FRAP and the Folin-Ciocalteu method. These findings depicted that leaf extract had a high presence of reducing compounds, which could produce higher yield of PMNPs. Numerous studies have also explained this fact that if extracts have higher antioxidant capacity and TPC, then it will show higher potential in producing PMNPs through the reduction of metal ions [35].

Characterization of Phylogenetic Magnetic Nanoparticles (PMNPs)

The fabrication of PMNPs was first confirmed through change in color from dark green to black using UV-vis absorption spectra [34]. Fig. 1 illustrates that the reaction between metal salt and plant extract was instantaneous and the color of the reaction solution changed from dark green to black (inset of Fig. 1) [34]. This fabrication might be explained in that a variety of plant bio-molecules (polyphenols) played a major role in the reduction of metal ions and sufficiently stabilized the Fe_3O_4 NPs to fabricate PMNPs under alkaline conditions (pH 12). Thus, after the reaction, it can be seen that the UV spectra of fabricated PMNPs had broad absorption at higher wavelength than plant extract, and there was no sharp absorption at lower wavelengths (Fig. 1(a, b)). The formation of PMNPs or the reactions that might occur in the fabrication of PMNPs are as shown in Equations:

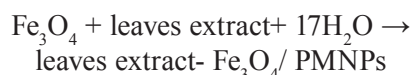
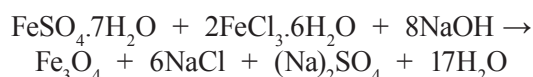


Fig. 2 illustrates the FTIR spectra of leaf extract and fabricated PMNPs. The FTIR spectra are revealing different peaks in the spectral range of $500\text{--}4000 \text{ cm}^{-1}$. These peaks were attributed to the probable presence of plant bio-molecules at the surface of PMNPs. Fig. 2 showed that the broad absorptions at 3454 cm^{-1} mainly represent the O-H stretching vibrations (polyphenolic group) and it was shifted to 3460 cm^{-1} (Fig. 2b). Its breadth might be due to the formation of intra and intermolecular hydrogen bonds [31]. The peaks at 2935 and 2893 cm^{-1} represent O-H stretching and C-H stretching vibrations of carboxylic acid, alcohol or alkene (Fig. 2b). A very strong peak at 1662 cm^{-1} revealed the presence of C=O stretching or C=C stretching vibration of acid derivatives and was shifted to 1639 cm^{-1} . These peaks indicated the sign of physisorbed or chemisorbed H_2O on the PMNPs [31, 32]. A slight broad absorption peak at 1163 cm^{-1} indicated the C-O stretching vibration of ester and it was shifted to 1114 cm^{-1} , indicating the C-O stretching vibration of aliphatic ether or bond of glucose ring in the extract. Moreover, after the reduction of metals salt solution, the prompt decrease in the intensity at 1662 and 1163 cm^{-1} implies the major role of the -OH group in this reduction process [20, 32]. Finally, a strong absorption band at 585 cm^{-1} indicates or can be attributed to the characteristic band of Fe-O, which suggests the formation of Fe_3O_4 NPs or PMNPs (as reported previously by Prasad et al. [32]). Therefore, FTIR results verified the capping and involvement of plant bio-molecules (polyphenol, carboxyl, glucose, alkene, primary amine, ester, aliphatic and ether) on the surface of PMNPs in the shape of -OH, C-H, C-O functional groups. In addition, the FTIR results also verified the results obtained from color development tests (as discussed in the extract characterization section).

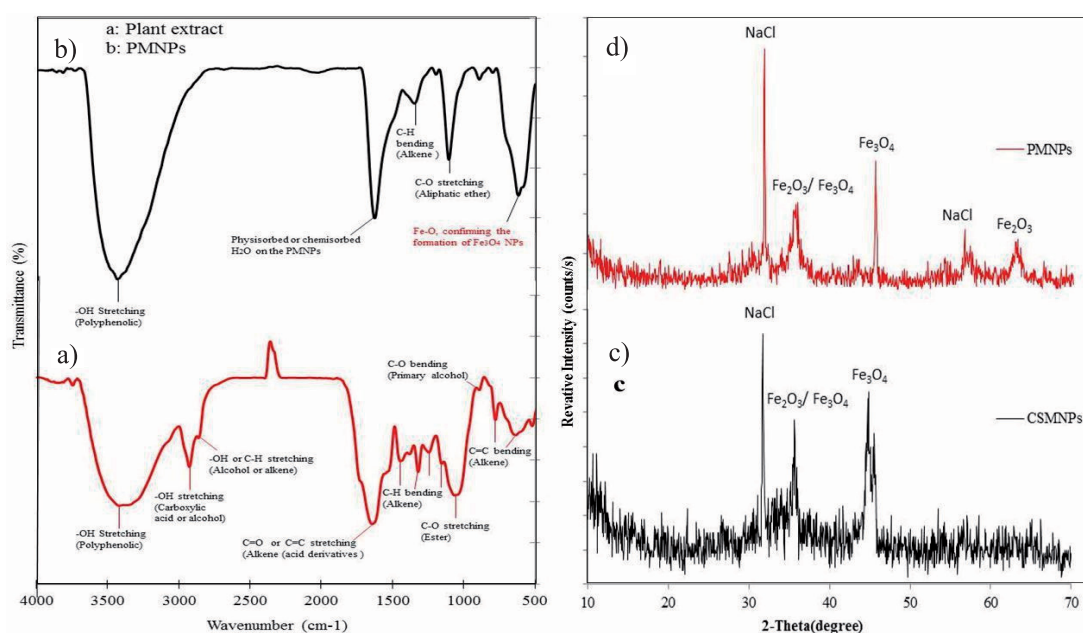


Fig. 2. Fourier transform infrared (FTIR) spectrum of a) plant extract and b) fabricated phyto-genic magnetic nanoparticles (PMNPs); and the powder XRD patterns of c) chemically synthesized magnetic nanoparticles (CSMNPs) and d) PMNPs.

Fig. 2d) shows the XRD pattern of the PMNP structure. The reflections in the XRD diagram were found to belong to iron oxide or magnetite (Fe_3O_4), ferric oxide or hematite (Fe_2O_3), in addition to NaCl [37]. The fabricated PMNPs were highly crystalline and the majority of them indicated the sign of magnetite/hematite NPs, and they could be clearly assigned to the cube shape of metallic iron. The results of XRD analysis showed a series of high characteristic diffraction peaks appearing at $2\theta = 32.5^\circ, 35.2^\circ, 45.4^\circ, 57.3^\circ$ and 62.8° , respectively. The peaks at $2\theta = 35.2^\circ$ and 62.8° mainly indicated the presence of iron oxide. The average diameter of the fabricated PMNPs was also calculated by using Scherres equation as $D = 0.89\lambda/\beta \cdot \cos\theta$, where D is the average particle size, λ is the wavelength of the $\text{CuK}\alpha$ irradiation, β belongs to the full width at half maximum intensity of the diffraction peak, and θ is the diffraction angle at $2\theta = 35.3^\circ$ peak of iron oxide NPs [35]. The fabricated PMNPs resulted in the mean crystallite size of $\sim 39\text{nm}$. For comparison, the XRD pattern of CSMNPs was also obtained in Fig. 2c). A more or less similar XRD pattern was observed, which also verified that our fabricated PMNPs contained magnetite and hematite of crystalline shapes. In addition, the XRD pattern of PMNPs was also matched with standard data for the pisumsativum peels extract of Fe_3O_4 NPs (JCPDS No. 82-1533), and the findings depicted that our fabricated PMNP diffraction peak was overlapping at $2\theta = 35.3^\circ$, thereby confirming the formation of Fe_3O_4 NPs [32].

Moreover, SEM analysis was carried out to observe the morphology of fabricated CSMNPs and PMNPs (Fig. 3). Fig. 3c) reveals that PMNPs mainly showed granular homogenous spherical shaped structure of Fe_3O_4

(magnetite) with diameter in the range of 30-50 nm. In contrast, CSMNPs were showing chain-like morphology (Fig. 3a). In addition, EDS/X analysis gives qualitative and as well as quantitative status of elements that might be implied in the fabrication of NPs. Fig. 3(b, d) shows that the EDX spectrum contained intense peaks of Na, Cl and C in addition to Fe and O. The Na and Cl peaks might have originated from NaOH and FeCl_2 precursors used in the fabrication of PMNPs and CSMNPs. The C peak in the case of PMNPs was attributed mainly to the polyphenol groups or other carbon-containing biomolecules that were present in the leaf extract (Fig. 7d). The findings revealed that the atomic percentages as obtained by EDX quantification were Fe (38.55%), C (5.92%), O (53.58%), Na (1.06%) and Cl (0.90%) in the case of CSMNPs (Fig. 7b). In contrast, the atomic percentages obtained for PMNPs were Fe (35.12%), C (17.12%), O (45.09%), Na (1.68%) and Cl (0.98%), which indicated that our fabricated PMNPs were keeping approximately a similar percentage of Fe and O, as we observed in the case of CSMNPs Fig. 3d). However, the percentages of C were higher than CSMNPs, which indicated the sign of the involvement of plant bio-molecules in the reduction of metal ions and stabilization of PMNPs (Fig. 3). Moreover, these values might be helpful in observing the atomic content on the surface and near-surface region of the fabricated PMNPs.

Removal Performance and Comparison

The effects of CV and EBT concentration were studied over the concentration range of 10-300 mg/L by keeping the dose constant at 0.500 g for both CSMNPs

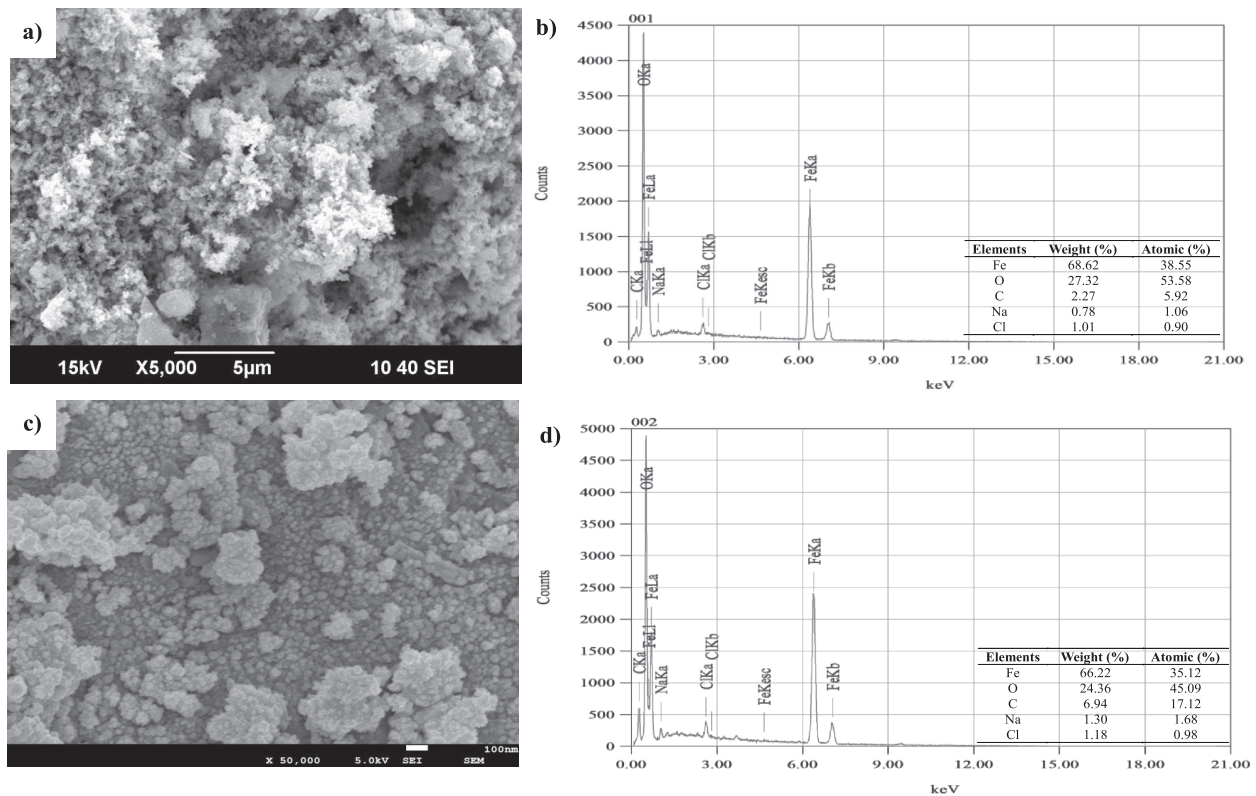


Fig. 3. Scanning electron microscopic (SEM) images and energy-dispersive X-ray (EDX) spectra of a) and b) chemically synthesized magnetic nanoparticles (CSMNPs) and c) and d) phytogetic magnetic nanoparticles (PMNPs).

and PMNPs. Throughout the experiments, the contact time was 540 min (9h) for both dyes. The changes in the concentration of CV and EBT at different contact times are shown in Figs 4 and 5. A complete degradation of CV was observed within 30 min of contact time for all concentrations, when CSMNPs were used (Fig. 4a). In contrast, a rapid but complete removal of CV was observed within 10min of contact time when PMNPs were used (Fig. 4b). In the case of EBT, a maximum of 97% removal efficiency was observed after the contact time of 540min and then it remained constant until the end of the experiment, when CSMNPs were used (Fig. 5a). In contrast, 100% removal efficiency of EBT was achieved within the first 10min of contact time, when PMNPs were used (Fig. 5b). The calculated percentage removal efficiency of the dyes at different concentrations and dosages is given in Table 1, which showed that the removal efficiency of CV and EBT appeared to be almost 100% over the entire concentration ranges, in case of PMNPs after contact time of 8 min, which reflects the effectiveness of PMNPs instead of CSMNPs. In contrast, in the case of CSMNPs, the percentage removal efficiency was less than 100 after the contact time of 8 min throughout all concentrations.

The kinetic experimental data were fitted to 1st- and 2nd-order rate equations. The equations were prepared by assuming the driving force of degradation to be proportional to the difference between the concentration

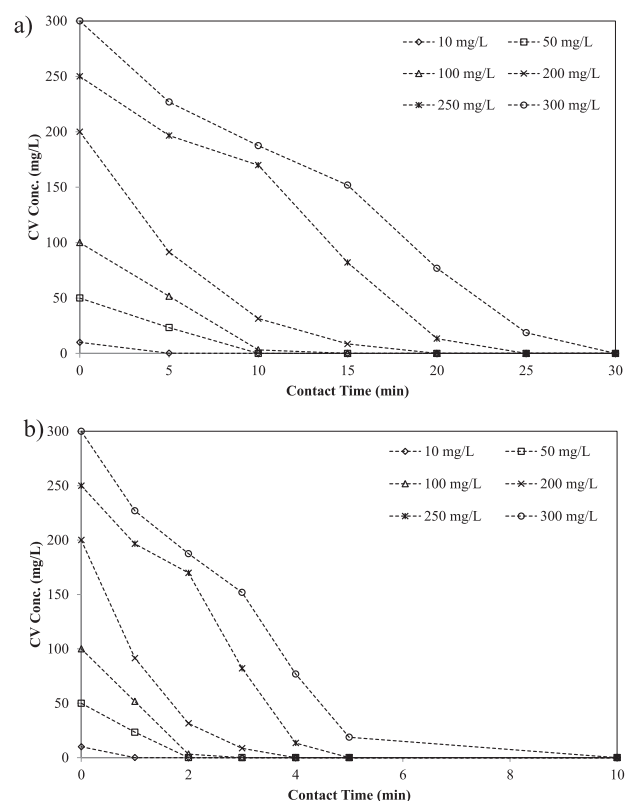


Fig. 4. Influence of contact time on the concentration of crystal violet (CV) at a) dosage: 0.5 g of chemically synthesized magnetic nanoparticles (CSMNPs); and b) dosage: 0.5 g of phytogetic magnetic nanoparticles (PMNPs).

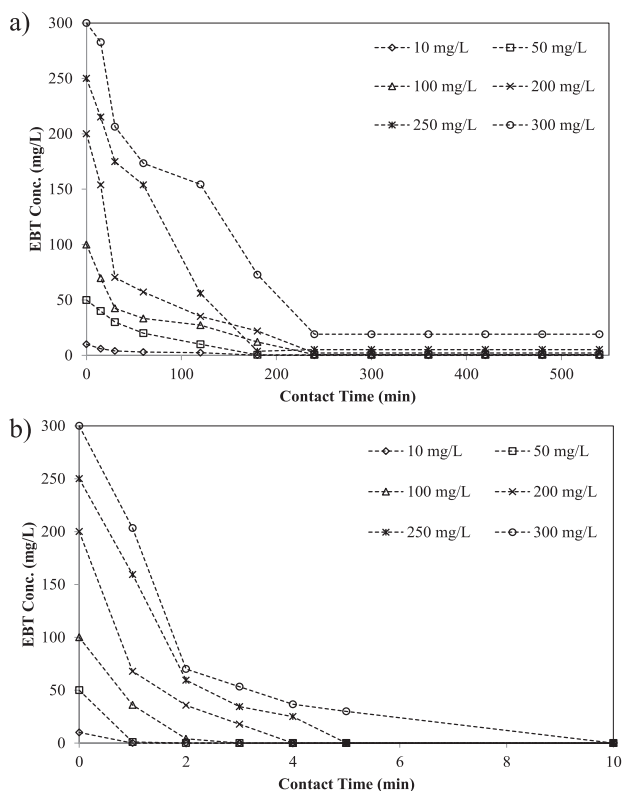


Fig. 5. Influence of contact time on the concentration of Eriochrome black T (EBT) at a) dosage: 0.5 g of chemically synthesized magnetic nanoparticles (CSMNPs); and b) dosage: 0.5 g of phylogenetic magnetic nanoparticles (PMNPs).

of dye (C_t) at any time prior to equilibrium and that with equilibrium (C_e). Thus, the 1st- and 2nd-order rate equations for the removal of solute from aqueous solution might be written as [20]:

First-order rate equation

$$-\frac{dC_t}{dt} = k_1(C_t - C_e)$$

Second order rate equation

$$-\frac{dC_t}{dt} = k_2(C_t - C_e)^2$$

... where C_t (mg/L) is the dye concentration in solution at time (t) and C_e (mg/L) is the dye concentration at equilibrium, and k_1 and k_2 are the rate constants for the 1st and 2nd equations.

$$\ln\left(\frac{C_t - C_e}{C_o - C_e}\right) = -k_1 t$$

$$\frac{1}{C_t - C_e} - \frac{1}{C_o - C_e} = k_2 t$$

...where C_o (mg/L) is the initial concentration of the dyes solution.

Table 1. Removal efficiency (%) of Crystal violet (CV) and Eriochrome black T (EBT) after contact time of 8 min at different initial concentrations; kinetics equilibrium data corresponding to the removal of CV and EBT at initial concentration of 300 mg/L (dosage: 0.5 g of chemically synthesized magnetic nanoparticles (CSMNPs) and phylogenetic magnetic nanoparticles (PMNPs)).

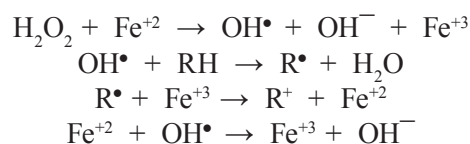
Dye name	Initial concentration of aqueous dyes solution (mg/L)					
	10	50	100	200	250	300
Removal efficiency (%) ±2.5%						
Chemically synthesized magnetic nanoparticles (CSMNPs)						
CV	97	53	48	45	31	20
EBT	60	57	51	47	39	31
Phylogenetic magnetic nanoparticles (PMNPs)						
CV	100	100	100	100	100	93
EBT	100	100	100	100	100	90
Kinetics equilibrium data						
Dye name	Removal efficiency (%) at equilibrium	Equilibrium time (min)	First order		Second order	
			k (min ⁻¹)	R ²	k (L/mg/min)	R ²
CSMNPs						
CV	100	30	0.01674	0.764	0.00107	0.158
EBT	97	540	0.01418	0.763	0.00023	0.044
PMNPs						
CV	100	10	0.01808	0.954	0.00107	0.035
EBT	100	10	0.01771	0.980	0.00158	0.009

These equations revealed that they can be used to explain the data corresponding to the pre-equilibrium stage (up to 30 min for CV and up to 250 min for EBT), when CSMNPs were used. On the other hand, up to 10 min time was adjusted for both dyes when PMNPs were employed. The results of linear regression analysis were used to calculate the rate constant for each dye. Table 1 shows the rate constants and corresponding linear correlation coefficient (R^2) values of CV and EBT at initial concentration of 300 mg/L, when CSMNPs and PMNPs were used. It can be observed that, according to the R^2 values, the degradation of CV and EBT seems to fit much better to 1st-order kinetics than 2nd-order for both CSMNPs and PMNPs. Similarly, the rate constant (k_1) values of CV and EBT (in the case of PMNPs) were higher than k_1 values of CV and EBT (in the case of CMNPs), which indicated faster degradation kinetics of CV and EBT for PMNPs.

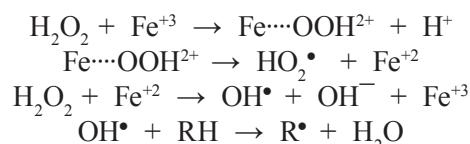
Overall, PMNPs appeared to be more effective than CSMNPs as a catalyst both in term of the extent and speed of dye degradation. The obtained results are summarized in Table 1 for CV and EBT. However, the CV degradation was much better than EBT in the case of CSMNPs. At this stage, it was not clear to what extent this could be related to the chemical nature of the CSMNPs or the oxidation state of the iron. Shahwan et al. [20] conducted a similar study for the degradation of methylene blue (MB) and methyl orange (MO) dyes from aqueous solution using green iron nanoparticles fabricated using green tea extract, and their performances were compared with chemically synthesized magnetic nanoparticles. The findings of this study revealed that green iron nanoparticles depicted better degradation performance and kinetics than chemically synthesized magnetic nanoparticles, and almost complete removal of MB dye was achieved after 200 min and 350 min for MO under experimental conditions. Similarly, almost 100% of MB was removed from solution within the contact time of 30 min [31]. In another study, 96% removal efficiency of MG was observed within the contact time of 60 min at 50 mg/L and 298K [33]. Recently, Prasad et al. [32] reported 96% removal of MO dye within the contact time of 60 min at a concentration of 100 mg/L. In comparison, our fabricated PMNPs performed comparatively much better to degrade CV and EBT within the contact time of 10 min in the concentration range 10-300 mg/L.

Proposed Removal Mechanism

Chemical oxidation is often considered a powerful way to remove or degrade toxic and organic pollutants from wastewaters. The oxidation is mainly dependent on the action of hydroxyl radical (OH^\bullet), which is produced by the traditional Fenton reagent in aqueous solution. Fenton reagent ($\text{Fe}^{+2}/\text{H}_2\text{O}_2$) is basically an amalgamation of Fe^{+2} ions and H_2O_2 in aqueous solution [38]. In the Fenton system, the production of (OH^\bullet) can be expressed as:



It can be observed that Fe^{+2} starts the reaction, leading to the generation of OH^\bullet , which further will attack the toxic and organic pollutants leading to their oxidation/degradation. On the other hand, in the Fenton-like system (i.e. $\text{Fe}^{+3}/\text{H}_2\text{O}_2$), the production of (OH^\bullet), can be explained as:



It can be seen that Fe^{+3} initiates the reaction instead of Fe^{+2} , which is being used in traditional Fenton processes and leads to the formation of $\text{Fe}\cdots\text{OOH}^{2+}$, which further will dissolve and generate Fe^{+2} , and these ferrous ions react with H_2O_2 to produce OH^\bullet , which further will attack the organic contaminants, leading to their oxidation/ degradation. Numerous studies show that Fe_3O_4 , FeOOH and $n\text{ZVI}$ can be employed as a source of Fe^{+2} ions in a Fenton-like process [39]. In addition, these materials are being used to catalyze oxidation of toxic dyes and other organic pollutants [40-43].

In our experiments, PMNPs were shown to contain Fe_3O_4 . Hence, the sustainability of the OH^\bullet production cycle will depend on the ease of Fe^{+2} ion availability. In this way, the surface of the Fe_3O_4 will first corrode in acidic medium, leading to the generation of Fe^{+2} ions, which further produce OH^\bullet radicals. Moreover, these generated OH^\bullet radicals then will attack the bonds in the dye molecules, which may be in solution or sorbed on the PMNP surface [44]. In this study, PMNPs showed greater degradation efficiency than CSMNPs if we compare with time. This reason might be explained in the sense that PMNPs had great potential to generate higher amounts of OH^\bullet radicals than CSMNPs at low pH, which was resultant to reducing the time required for complete degradation.

It was also observed that by adding H_2O_2 solution to the dye solution, the pH of the dye solution (containing PMNPs) was reduced to 3.52 (in the case of CV) and 3.41 (in the case of EBT), and it continued to decrease up to 3.04 and 3.01 for CV and EBT, respectively, at the end of the experiments – despite the fact that initially we adjusted dye solution pH at 6.5. We calculated pH at the start and end of the each experiment. Importantly, it has been reported in many studies that if pH of the solution is less than 4, then the ease of generation of OH^\bullet radicals will increase, thus increasing the degradation efficiency of the Fenton system [45]. In our experiments, the pH values measured (at the end of the experiments) was less than 4.0, which

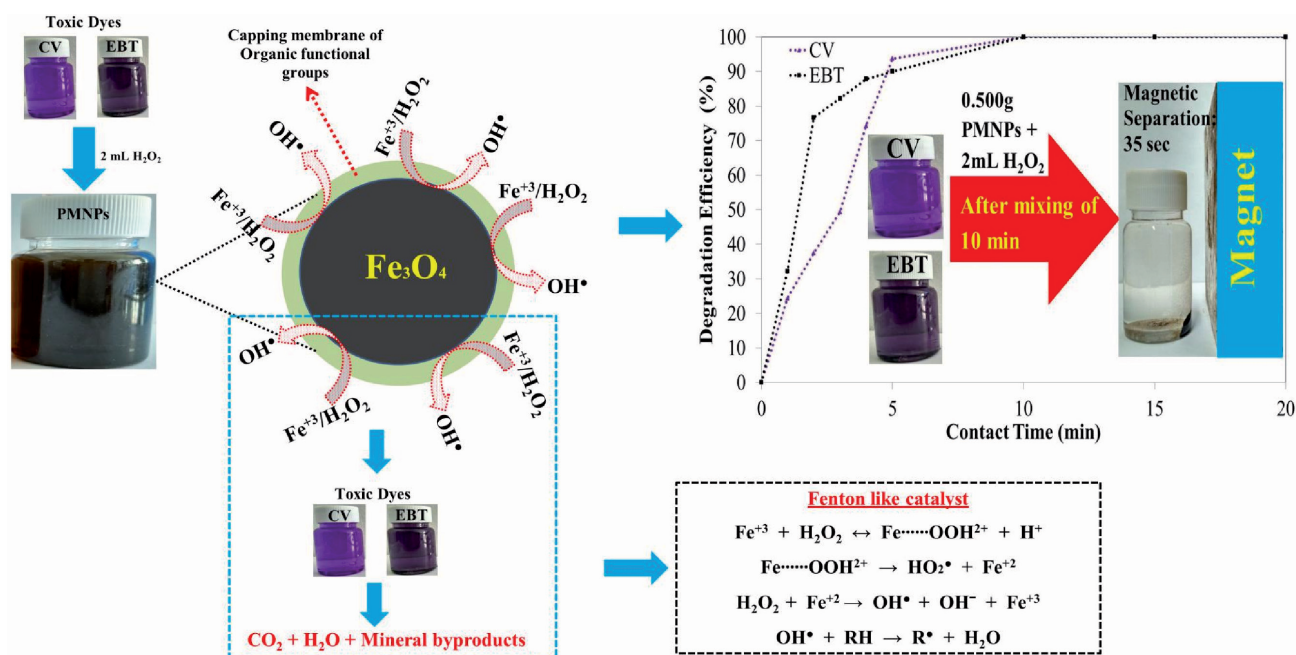


Fig. 6. Proposed removal mechanism of Crystal violet (CV) and Eriochrome black T (EBT) by phytogetic magnetic nanoparticles (PMNPs) in the presence of 2 mL (30%) H_2O_2 .

was also an important factor for the generation of higher OH^{\bullet} radicals and reducing the degradation time up-to 10 min for both dyes. Therefore, in this study, PMNPs were mainly showing a Fenton-like mechanism to degrade toxic and aromatic pollutants under acidic conditions ($\text{pH} < 4.0$) because Fe_3O_4 was mainly used as a source of Fe^{+2} ions to produce OH^{\bullet} radicals for the

oxidation of toxic dyes. Furthermore, the FTIR, XRD and EDX analysis have already verified the presence of iron oxide in PMNPs. The relatively weak and broad peaks in the XRD diagram indicated that PMNPs had amorphous grains, which might be a factor that will assist PMNP dissolution under the acidic medium, and the generation of Fe^{+2} ions will increase with the decrease

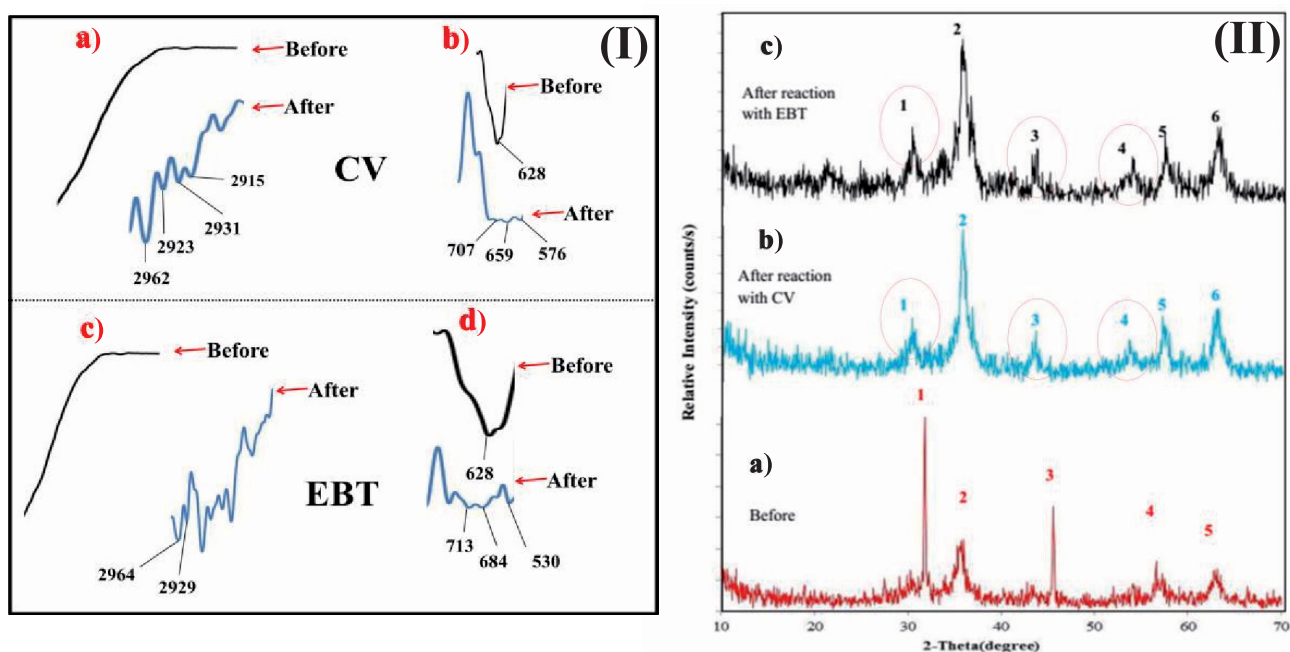


Fig. 7. Fourier transform infrared (FTIR) spectrum of phytogetic magnetic nanoparticles (PMNPs) a) and b) before and after reaction with Crystal violet (CV); c) and d) before and after reaction with Eriochrome black T (EBT); (II) the powder XRD patterns of a) PMNPs, b) after reaction with CV and c) after reaction with EBT.

in pH. It is also worth mentioning that the reusability of the PMNPs was greatly damaged by adding H_2O_2 solution into the dye solution because capping of plant bio-molecules disappeared due to the action of OH^\bullet radicals. This phenomenon is also supporting the fact that Fe_3O_4 was corroded from the surface of PMNPs, which further was employed in the generation of OH^\bullet radicals leading to the degradation of toxic dyes (Fig. 6).

Fourier Transforms Infrared Spectroscopic (FTIR) and Powder X-ray Diffraction (XRD) Analyses

The FTIR spectra were also studied after the degradation reaction of CV and EBT dyes. The FTIR profile obtained after the reaction with CV and EBT showed prominent spectral attributes in the range of 296 to 2915 cm^{-1} (Fig. 7(I)). These peaks were mainly associated to the stretching vibration of $-CH_3$ and C-H of the methyl groups, created from CV and EBT and/or its products sorbed on the surface of PMNPs. Moreover, other peaks also appeared in the range of 713-530 cm^{-1} , which were related to $-C-S-$ stretching vibration (Fig. 7(I)). These peaks were also showing that the degradation products were sorbed or attached to the surface of PMNPs. Similarly, the XRD pattern was also studied after the reaction with CV and EBT. The results clearly indicated that new peaks originated at $2\theta = 30^\circ, 44.2^\circ$ and 57.2° , in addition to other subsisted peaks (Fig. 7(II)). While the intensities of remaining peaks were increased slightly and expanded, this indicates the dissolution of PMNPs under acid attack (Fig. 7(II)). The occurrence of new peaks and increments in the intensities might be an indication of degradation by PMNPs. In addition, the concentration of total organic carbon (TOC) and total nitrogen (TN) was also simultaneously measured by combining the Shimadzu total organic carbon analyzer (TOC-V, Shimadzu Scientific Instruments, Inc., USA) and the TN measurement unit (TNM-1, Shimadzu Scientific Instruments, Inc., USA) before and after adding PMNPs from both dye solutions. It was noticed that initially the concentration of TOC and TN was 48.5 ± 2 and 86.26 ± 2 mg/L, respectively, in both dye solutions. Later, it was significantly dropped (from 48.5 ± 2 to 1.58 ± 1.5 mg/L for TOC and 86.26 ± 2 to 3.5 ± 1.8 mg/L for TN) after adding PMNPs and H_2O_2 in both dye solutions.

Conclusions

Overall, to the best of our knowledge, for the first time innovative PMNPs were produced by employing a non-toxic, cheap and environmental friendly "green" recipe using leaf extract of *F. chinensis Roxb* as reducing and capping agent. The developed methods did not require any additional toxic or hazardous chemicals and can be scaled up to bulk level. The formation of PMNPs was characterized with the help of different

techniques, i.e., UV-visible spectra, FTIR, powder XRD, SEM and EDX. The FTIR analysis depicted the presence of plant bio-molecules (polyphenols, carboxyl, reducing sugars, flavonoids and organic acids) in the leaf extract, which were responsible for the bio-reduction of metal ions and the stabilization of PMNPs. Furthermore, the powder XRD analysis results confirmed the presence of iron oxide or magnetite (Fe_3O_4) NPs having crystalline cube shape of metallic iron. Similarly, SEM analysis indicated that PMNPs mainly showed granular homogenous porous spherical-shaped structure of Fe_3O_4 (magnetite) with diameter in the range of 30-50 nm. In addition, EDX results showed the presence of higher percentages of carbon, which clearly indicated the sign of the involvement of plant bio-molecules in the reduction of metal ions and stabilization of PMNPs. Furthermore, the results indicated that our fabricated PMNPs demonstrated impressive removal capabilities and the kinetics compared to CSMNPs in the presence of H_2O_2 for toxic dyes (CV and EBT) from aqueous solutions and acted as a Fenton-like catalyst. A complete 100% degradation efficiency of CV and EBT was achieved within the contact time of 10 min and the kinetic experimental data fit well with the first-order degradation rate equation for both dyes. Altogether, the developed "green" recipe can easily be implemented to produce potentially biocompatible and non-toxic magnetic nanoparticles for wastewater treatment.

Acknowledgements

This work was supported by the State Key Laboratory of Environmental Criteria and Risk Assessment (No. SKLECRA 2013FP12) and Shandong Province Key Research and Development Program (2016GSF115040). The first author would like to thank the Chinese Scholarship Council (CSC No. 2016GXYO20) for its financial support.

Conflict of Interest

The authors declare no conflict of interest.

References

1. ALI I., KHAN Z.M., SULTAN M., MAHMOOD M.H., FARID H.U., ALI M., NASIR A. Experimental Study on Maize Cob Trickling Filter-Based Wastewater Treatment System: Design, Development, and Performance Evaluation. *Pol. J. Environ. Stud.* **25** (6), 2265, **2016**.
2. ALI I., PENG C., NAZ I., KHAN Z.M., SULTAN M., ISLAM T., ABBASI I.A. Phyto-genic magnetic nanoparticles for wastewater treatment: a review. *RSC Adv.* **2017**, 7, 40158, **2017a**.
3. ALI I., PENG C., KHAN Z.M., NAZ I. Yield cultivation of magnetotactic bacteria and magnetosomes: A review. *J. Basic Microbiol.* **9999**, 1, **2017b**.

4. ALI I., KHAN Z.M., PENG C., NAZ I., SULTAN M., ALI M., MAHMOOD M.H., NIAZ Y. Identification and Elucidation of the Designing and Operational Issues of Trickling Filter Systems for Wastewater Treatment. *Pol. J. Environ. Stud.* **26** (6), 2431, **2017c**.
5. FARID H.U., BAKHSH A., ALI M.U., MAHMOOD-KHAN Z., SHAKOOR A., ALI I. Field investigation of aquifer storage recovery (ASR) technique to recharge groundwater: a case study in Punjab province of Pakistan. *Water Sci. Tech-W. Sup.p.w.s* 2017083, **2017**.
6. PUNRATTANASIN P., SARIEM P. Adsorption of copper, zinc, and nickel using loess as adsorbents. *Pol. J. Environ. Stud.* **24**, 1259, **2015**.
7. SUROVKA D., PERTILE E. Sorption of Iron, Manganese, and Copper from Aqueous Solution Using Orange Peel: Optimization, Isothermic, Kinetic, and Thermodynamic Studies. *Pol. J. Environ. Stud.* **26** (2), 795, **2017**.
8. TĂNASE A.M., CHICIUDEAN I., MEREUȚĂ I., IONESCU R., CORNEA C.P., VASSU T., STOICA I. Microbial Community Dynamics in Field-Scale Biopile Bioremediation. *Pol. J. Environ. Stud.* **26** (1), 331, **2017**.
9. PALIULIS D. Removal of formaldehyde from synthetic wastewater using natural and modified zeolites. *Pol. J. Environ. Stud.* **25** (1), 251, **2017**.
10. VAKILI M., RAFATULLAH M., SALAMATINIA B., ABDULLAH A.Z., IBRAHIM M.H., TAN K.B., GHOLAMI Z., AMOUZGAR P. Application of chitosan and its derivatives as adsorbents for dye removal from water and wastewater: A review. *Carbohydr. Polym.* **113**, 115, **2014**.
11. YAGUB M.T., SEN T.K., AFROZE S., ANG H.M. Dye and its removal from aqueous solution by adsorption: a review. *Adv. Colloid Interface Sci.* **209**, 172, **2014**.
12. CRINI G. Non-conventional low-cost adsorbents for dye removal: a review. *Bioresour. Technol.* **97** (9), 1061, **2006**.
13. SIVARAJ R., NAMASIVAYAM C., KADIRVELU K. Orange peel as an adsorbent in the removal of acid violet 17 (acid dye) from aqueous solutions. *Waste management*, **21** (1), 105, **2001**.
14. LAKSHMI U.R., SRIVASTAVA V.C., MALL I.D., LATAYE D.H. Rice husk ash as an effective adsorbent: Evaluation of adsorptive characteristics for Indigo Carmine dye. *J. Environ. Manag.* **90** (2), 710, **2009**.
15. GONG R., DING Y., LI M., YANG C., LIU H., SUN Y. Utilization of powdered peanut hull as biosorbent for removal of anionic dyes from aqueous solution. *Dyes Pigm.* **64** (3), 187, **2005**.
16. NAMASIVAYAM C., KUMAR M.D., SELVI K., BEGUM R.A., VANATHI T., YAMUNA R.T. 'Waste'coir pith – a potential biomass for the treatment of dyeing wastewaters. *Biomass Bioenergy*. **21** (6), 477, **2001**.
17. PORKODI K., KUMAR K.V. Equilibrium, kinetics and mechanism modeling and simulation of basic and acid dyes sorption onto jute fiber carbon: Eosin yellow, malachite green and crystal violet single component systems. *J. Hazard. Mater.* **143** (1), 311, **2007**.
18. SIVASHANKAR R., SATHYA A.B., VASANTHARAJ K., SIVASUBRAMANIAN V. Magnetic composite an environmental super adsorbent for dye sequestration – A review. *ENMM*. **1**, 36, **2014**.
19. LUO X., ZHANG L. High effective adsorption of organic dyes on magnetic cellulose beads entrapping activated carbon. *J. Hazard. Mater.* **171** (1), 340, **2009**.
20. SHAHWAN T., SIRRIAH S.A., NAIRAT M., BOYACI E., EROĞLU A.E., SCOTT T.B., HALLAM K.R. Green synthesis of iron nanoparticles and their application as a Fenton-like catalyst for the degradation of aqueous cationic and anionic dyes. *Chem. Eng. J.* **172** (1), 258, **2011**.
21. SU C. Environmental implications and applications of engineered nanoscale magnetite and its hybrid nanocomposites: A review of recent literature. *J. Hazard. Mater.* **322**, 48, **2017**.
22. SHAMAILA S., SAJJAD A.K.L., FAROOQI S.A., JABEEN N., MAJEED S., FAROOQ I. Advancements in nanoparticle fabrication by hazard free eco-friendly green routes. *Appl. Mater. Today*. **5**, 150, **2016**.
23. MYSTRIOTI C., SPARIS D., PAPASIOPI N., XENIDIS A., DERMATAS D., CHRYSOCHOOU M. Assessment of polyphenol coated nano zero valent iron for hexavalent chromium removal from contaminated waters. *Bull. Environ. Contam. Toxicol.* **94**, 302, **2015**.
24. FAZLZADEH M., RAHMANI K., ZAREI A., ABDOALLAHZADEH H., NASIRI F., KHOSRAVI R. A novel green synthesis of zero valent iron nanoparticles (NZVI) using three plant extracts and their efficient application for removal of Cr (VI) from aqueous solutions. *Adv. Powder Technol.* **28**, 122, **2017**.
25. GUPTA V.K., NAYAK A. Cadmium removal and recovery from aqueous solutions by novel adsorbents prepared from orange peel and Fe₂O₃ nanoparticles. *Chem. Eng. J.* **180**, 81, **2012**.
26. LINGAMDINNE L.P., CHANG Y.Y., YANG J.K., SINGH, J., CHOI E.H., SHIRATANI M., ATTRI P. Biogenic reductive preparation of magnetic inverse spinel iron oxide nanoparticles for the adsorption removal of heavy metals. *Chem. Eng. J.* **307**, 74, **2017**.
27. MARTÍNEZC M., LÓPEZG M., BARRIADA J.L., HERRERO R., VICENTE M.E.S. Green synthesis of iron oxide nanoparticles. Development of magnetic hybrid materials for efficient As (V) removal. *Chem. Eng. J.* **301**, 83, **2016**.
28. PRASAD K.S., GANDHI P., SELVARAJ K. Synthesis of green nano iron particles (GnIP) and their application in adsorptive removal of As (III) and As (V) from aqueous solution. *Appl. Surf. Sci.* **317**, 1052, **2014**.
29. VENKATESWARLU S., KUMAR B.N., PRATHIMA B., SUBBARAO Y., JYOTHI N.V.V. A novel green synthesis of Fe₃O₄ magnetic nanorods using Punica Granatum rind extract and its application for removal of Pb(II) from aqueous environment. *Arab. J. Chem.* **2014**.
30. VENKATESWARLU S., LEE D., YOON M. Bioinspired 2D-Carbon Flakes and Fe₃O₄ Nanoparticles Composite for Arsenite Removal. *ACS Appl. Mater. Interfaces.* **8** (36), 23876, **2016**.
31. BUAZAR F., BAGHLANIN M.H., BADRI M., KASHISAZ M., KHALEDIN A., KROUSHAWI F. Facile one pot phytosynthesis of magnetic nanoparticles using potato extract and their catalytic activity. *Starch/Staerke.* **68** (7-8), 796, **2016**.
32. PRASAD C., YUVARAJA G., VENKATESWARLU P. Biogenic synthesis of Fe₃O₄ magnetic nanoparticles using Pisum sativum peels extract and its effect on magnetic and Methyl orange dye degradation studies. *J. Magn. Mater.* **424**, 376, **2017**.
33. WENG X., HUANG L., CHEN Z., MEGHARAJ M., NAIDU R. Synthesis of iron-based nanoparticles by green tea extract and their degradation of malachite. *Ind. Crops Prod.* **51**, 342, **2013**.
34. ALI I., PENG C., YE T., NAZ I. Sorption of cationic malachite green dye on phyto-genic magnetic nanoparticles functionalized by 3-mercaptopropanoic acid. *RSC Adv.* **8**, 8878, **2018**.

35. WEI Y., FANG Z., ZHENG L., TSANG E.P. Biosynthesized iron nanoparticles in aqueous extracts of *Eichhorniacrassipes* and its mechanism in the hexavalent chromium removal. *Appl. Surf. Sci.* **399**, 322, **2017**.
36. SMULEAC V., VARMA R., SIKDAR S., BHATTACHARYYA D. Green synthesis of Fe and Fe/Pd bimetallic nanoparticles in membranes for reductive degradation of chlorinated organics. *J. Membr. Sci.* **379** (1), 131, **2011**.
37. NASRAZADANI S., NAMDURI H. Study of phase transformation in iron oxides using laser induced breakdown spectroscopy. *Spectrochim. Acta B Atomic Spectrosc.* **61** (5), 565, **2006**.
38. MOON B.H., PARK Y.B., PARK K.H. Fenton oxidation of Orange II by pre-reduction using nanoscale zero-valent iron. *Desalination.* **268** (1), 249, **2011**.
39. XUE X., HANNA K., DENG N. Fenton-like oxidation of Rhodamine B in the presence of two types of iron (II, III) oxide. *J. Hazard. Mater.* **166** (1), 407, **2009**.
40. SHIN S., YOON H., JANG J. Polymer-encapsulated iron oxide nanoparticles as highly efficient Fenton catalysts. *Catal. Commun.* **10** (2), 178, **2008**.
41. XU L., WANG J. A heterogeneous Fenton-like system with nanoparticulate zero-valent iron for removal of 4-chloro-3-methyl phenol. *J. Hazard. Mater.* **186** (1), 256, **2011**.
42. SHU H.Y., CHANG M.C., CHEN C.C., CHEN P.E. Using resin supported nano zero-valent iron particles for decoloration of Acid Blue 113 azo dye solution. *J. Hazard. Mater.* **184** (1), 499, **2010**.
43. KALLEL M., BELAID C., MECHICHI T., KSIBI M., ELLEUCH B. Removal of organic load and phenolic compounds from olive mill wastewater by Fenton oxidation with zero-valent iron. *Chem. Eng. J.* **150** (2), 391, **2009**.
44. WATTS R.J., FOGET M.K., KONG S.H., TEEL A.L. Hydrogen peroxide decomposition in model subsurface systems. *J. Hazard. Mater.* **69** (2), 229, **1999**.
45. KUO W.G. Decolorizing dye wastewater with Fenton's reagent. *Water Res.* **26** (7), 881, **1992**.